Step-Controlled Strain Relaxation in the Vicinal Surface Epitaxy of Nitrides

X. R. Huang,[1,*] J. Bai,[1] M. Dudley,[1] B. Wagner,[2] R. F. Davis,[2] and Y. Zhu[3]

[1]*Department of Materials Science and Engineering, State University of New York at Stony Brook, Stony Brook, New York 11794-2275, USA*

[2]*Department of Materials Science and Engineering, North Carolina State University, Raleigh, North Carolina 27695-7907, USA*

[3]*Materials Science Department, Brookhaven National Laboratory, Upton, New York 11973, USA*

(Received 8 November 2004; revised manuscript received 22 February 2005; published 17 August 2005)

On-axis and vicinal GaN/AlN/6*H*-SiC structures grown under identical conditions have been studied by x-ray diffraction and transmission electron microscopy to demonstrate the distinctive features of vicinal surface epitaxy (VSE) of nitrides on SiC. In VSE, the epilayers are tilted from the substrate due to the out-of-plane lattice mismatch (Nagai tilts), and the in-plane mismatch strains are more relaxed. The majority of misfit dislocations (MDs) at the vicinal AlN/6*H*-SiC interface are found to be *unpaired* partial MDs that are geometrically necessary to correct the stacking sequences from 6*H* to 2*H*. This mechanism indicates that it is possible to develop ''step-controlled-epitaxy'' strategies to control strain relaxation by adjusting the substrate offcut angles.

DOI: 10.1103/PhysRevLett.95.086101 PACS numbers: 68.55.Jk, 61.72.Dd, 68.47.Fg, 68.55.Ac

In epitaxy of nitrides on SiC or sapphire, it is advantageous to make the mismatch strains relax quickly near the interface so as to achieve in the following growth a nearly strain-free epilayer. For epitaxy of GaN, the epilayer thickness required for full strain relaxation can be up to a few micrometers and the strains tend to be relaxed gradually [1], leading to gradients of lattice spacings, which may result in inhomogeneous electronic states and a high density of defects in the epilayer. Therefore, it is desirable to explore strategies for rapidly relaxing mismatch strains within a narrow thickness. Vicinal surface epitaxy (VSE) may be such a scheme.

VSE has been reported as a promising technique that can significantly improve the crystalline quality of nitrides grown on SiC or sapphire [2–6]. For example, Xie *et al.* [3] demonstrated that VSE can suppress the formation of threading dislocations (TDs) by one and two orders for the edge and screw types, respectively. As the underlying mechanisms are far from completely understood, however, VSE has not attracted enough attention. In this Letter, we use high-resolution x-ray diffraction (HRXRD) and transmission electron microscopy (TEM) to study GaN/AlN epilayers grown on on- and off-axis 6*H*-SiC(0001) substrates and to demonstrate the distinctive features of nitride VSE. These features reveal a novel strain relaxation mechanism in which the 2*H*/6*H* interface steps provide natural sites for the nucleation of misfit dislocations (MDs).

We focus on two GaN/AlN/6*H*-SiC samples grown under identical growth conditions (side by side in the reactor). The 6*H*-SiC substrate of sample 1 has a (0001) surface (miscut $<0.1°$ in the synchrotron Laue pattern) while sample 2 was offcut by 3.5° toward $[11\bar{2}0]$. Both samples consist of a 1 μm GaN epilayer grown by low pressure metal-organic chemical vapor deposition at 1020 °C and a 0.1 μm AlN buffer layer grown at 1100 °C. HRXRD was conducted on a Bede D1 diffractometer, and TEM was performed on a JEOL JEM 3000F system.

The full width at half maximum (FWHM) values of the GaN 0002 rocking curves for samples 1 and 2 are 292″ and 139″ (arc sec), respectively, while for the glancing-incidence GaN $11\bar{2}4$ reflections, the two FWHMs are 363″ and 220″. Obviously, the GaN epilayer of sample 2 has higher crystalline quality. In the reciprocal space map, the GaN 0002, SiC 0006, and AlN 0002 peaks of sample 1 are perfectly aligned along [0001], indicating that the average orientations of the GaN, AlN, and SiC (0001) basal planes are exactly parallel. In contrast, the three peaks of sample 2 are displaced from each other along $[11\bar{2}0]$, indicating epitaxial tilts.

A triple-axis ω-2θ scan (d-spacing scan along [0001]) of sample 1 is shown in Fig. 1(a). For sample 2, three ω-2θ scans passing through the GaN, SiC, and AlN peak centers, respectively, were measured, as plotted together in Fig. 1(b). The AlN c (bilayer) lattice parameters determined from Fig. 1 are $c^1_{\mathrm{AlN}} = 2.498\,84$ and $c^2_{\mathrm{AlN}} = 2.493\,58$ Å based on $c_{6H\text{-SiC}} = 2.519\,96$ and $a_{6H\text{-SiC}} = 3.081\,29$ Å [7]. In terms of the strain-free parameters $c_{\mathrm{AlN}} = 2.491$ and $a_{\mathrm{AlN}} = 3.112$ Å [2], the AlN layers of both samples are under tension along [0001], but the strain $\varepsilon^2_{zz}(= c^2_{\mathrm{AlN}}/c_{\mathrm{AlN}} - 1) = 1.04 \times 10^{-3}$ is only $\sim 1/3$ of ε^1_{zz}. Weak diffraction of the AlN layers prevents us from directly measuring their a parameters from asymmetric reflections, but, based on the biaxial strain model, the AlN layers could be compressed in the basal plane, and the ratio between the two in-plane strains ε^2_{xx} and ε^1_{xx} is also 1/3; i.e., the vicinal AlN layers of sample 2 are more relaxed. The c parameters of the GaN films derived from Fig. 1 are $c^1_{\mathrm{GaN}} = 2.595\,12$ and $c^2_{\mathrm{GaN}} = 2.591\,76$ Å. Based on the strain-free parameters $c_{\mathrm{GaN}} = 2.5932$ and $a_{\mathrm{GaN}} = 3.1890$ Å [8], we have $c^1_{\mathrm{GaN}} > c_{\mathrm{GaN}} > c^2_{\mathrm{GaN}}$. Asymmetric reflections show that the GaN layer of sample 1 has a

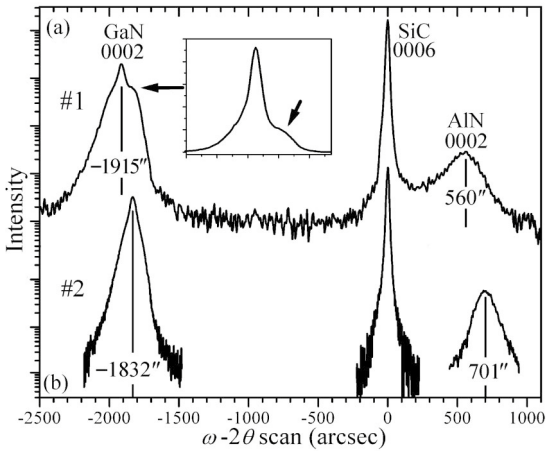

FIG. 1. Triple-axis ω-2θ scans showing the c lattice constant differences. The SiC 0006 peak positions are set to 0. Inset shows the secondary GaN peak of sample 1 at linear intensity scale.

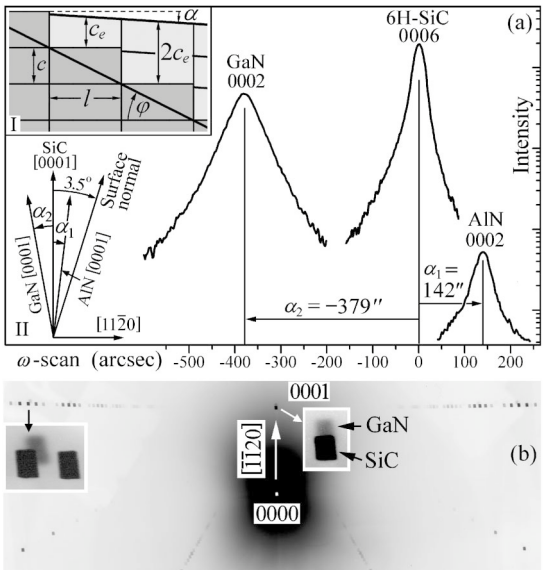

FIG. 2. Nagai tilts in sample 2. (a) Triple-axis ω scans. Inset I: origin of Nagai tilt. Inset II: tilt configuration. (b) Backreflection synchrotron Laue pattern recorded with the incident beam perpendicular to the crystal surface and the x-ray film. Sample-to-film distance 25.4 cm, 0000-to-0001 distance 31.2 mm, 0001 spot splitting 0.9 mm.

compressive strain $\varepsilon^1_{xx\mathrm{GaN}} = -2.24 \times 10^{-3}$. In contrast, the GaN layer of sample 2 is under tension with $\varepsilon^2_{xx\mathrm{GaN}} = 1.17 \times 10^{-3}$.

The tensile strain usually results from the thermal expansion coefficient difference, $\sim 1.4 \times 10^{-6}$ K^{-1} [2], between SiC (or AlN) and GaN. This implies that the GaN epilayer of sample 2 was fully relaxed at the growth temperature, while that of sample 1 had an in-plane strain of $\sim -4 \times 10^{-3}$. The arrow at the secondary peak in Fig. 1(a) shows that the on-axis GaN film roughly consists of two regions: the lower region is strained (corresponding to the main 0002 peak) while the thin top layer is fully relaxed as the secondary peak position coincides with the GaN peak position in Fig. 1(b). In comparison, sample 2 has a uniform lattice constant in the GaN epilayer as indicated by the sharper GaN peak in Fig. 1(b). Obviously, VSE can facilitate rapid and smooth strain relaxation at the interface.

Figure 2(a) shows the triple-axis ω scans (orientation scans) of the GaN 0002, SiC 0006, and AlN 0002 peak centers. These curves reveal that the basal planes of AlN and GaN in sample 2 are tilted from the substrate by $\alpha_1 = 142'' \pm 5''$ and $\alpha_2 = -370'' \pm 5''$, respectively, along the [11$\bar{2}$0] offcut direction (see inset II). Interestingly, these tilts can be explained by the simple Nagai model in inset I, which relates the tilt angle α with the offcut angle φ by $\tan\alpha = -(\Delta c/c)\tan\varphi$, where $\Delta c = c_e - c$ [9]. The $\Delta c/c$ values measured above for AlN/SiC and GaN/AlN are -1.05% and 3.94%, respectively. With $\varphi = 3.5°$, the tilt between AlN and SiC is then $\alpha'_1 = 134''$ while that between GaN and AlN is $-497''$ according to the Nagai equation. The GaN layer thus has a tilt of $\alpha'_2 = -363''$ with respect to the substrate. These results are consistent with the measured tilts $142''$ and $-370''$. Note that if the AlN buffer did not exist, the tilt of the GaN layer grown directly on the vicinal SiC(0001) surface would be $-360''$ according to the Nagai equation, very close to the measured value of $-363''$ in Fig. 2. This indicates that the AlN surface preserves the average surface morphology of the substrate. The tilt configuration of sample 2 can be seen more clearly from the synchrotron Laue pattern in Fig. 2(b), where two slightly displaced patterns diffracted from SiC and GaN, respectively, are present (while the AlN pattern is too weak to be observed). Here the splitting of the 0001 spot purely results from the tilt between the GaN and SiC (0001) planes. Figure 2(b) also verifies that the tilt direction is toward [$\overline{1}\overline{1}$20].

For GaN grown on offcut sapphire substrates ($\varphi < 2°$), we also found that the epitaxial tilt follows the Nagai model [10]. It has been found that the Nagai model is not applicable for nonpseudomorphic zinc-blende-type (001) heterostructures where the 60° MDs have [001] Burgers vector components that can result in extra lattice tilts or mosaicity [11,12]. Here despite the large mismatch, the strains in vicinal nitrides are apparently relaxed by basal MDs with *pure in-plane Burgers vectors.*

To understand the underlying mechanisms, high-resolution TEM (HRTEM) has been applied to study the microstructures of the epilayers and interfaces. A typical HRTEM cross-section image recorded at the AlN/SiC interface of the vicinal sample 2 is shown in Fig. 3(a). Figure 3(b) is the 11$\bar{2}$0 filtered image, which reveals three MDs with the extra half planes located in the SiC substrate. The 0004 filtered image in Fig. 3(c) shows no vertical lattice displacement around the MDs. Therefore, the Burgers vectors of the MDs must lie in the basal plane, consistent with the Nagai tilt. Such MDs have been observed in all the (1$\bar{1}$00) TEM specimens cut from sample 2, and they are the main defects at the AlN/SiC interface. In

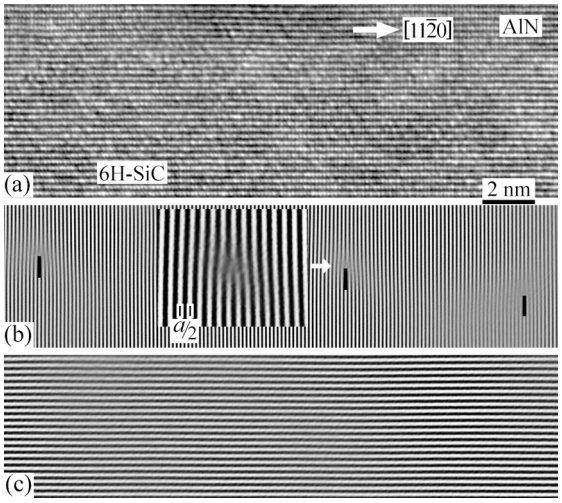

FIG. 3. (a) The $[1\bar{1}00]$ projection HRTEM image of the AlN/6*H*-SiC interface in sample 2. (b),(c) Filtered images from masked fast Fourier transformation of (a) showing the GPMDs. (b) $\mathbf{g} = 11\bar{2}0$. (c) $\mathbf{g} = 0004$.

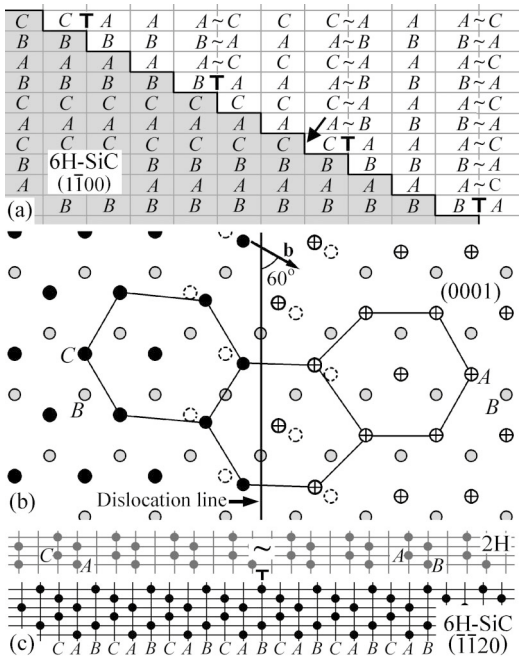

FIG. 4. (a) Formation of GPMDs at the mismatched interface steps. (b) Gradual transition of the stacking sequence of the AlN lattice for a 60° GPMD connecting the *A* and *C* stacking bilayers on a *B* bilayer. Dashed circles represent the original stacking positions without deformation. (c) The $[11\bar{2}0]$ view of the gradual stacking sequence change above a GPMD with no vertical boundary.

contrast, the average MD density in sample 1 is less than half of that in sample 2.

In Fig. 3(b), the projections of the MD Burgers vectors onto the $(1\bar{1}00)$ plane are all $a/2$. As the dislocations are along $[1\bar{1}00]$, the MDs can be only 30° complete dislocations (with Burgers vectors $\pm\frac{1}{3}[\bar{2}110]$ or $\pm\frac{1}{3}[11\bar{2}0]$) or 60° partials. Since the former is energetically unreasonable, the MDs should be 60° partials. In Fig. 3(b), however, the MDs are generally located on different terraces, indicating that these MDs are *unpaired* partials rather than paired partials dissociated from complete dislocations. The existence of high-density unpaired partials is surprising, but it can be explained in Fig. 4.

Figure 4(a) shows a possible periodic configuration of a 2*H* wurtzite structure epitaxially grown on a stepped 6*H*-SiC (0001) surface [13]. Because of the two different structures, mismatched stacking sequences exist at the interface, and they can be corrected either by the formation of prismatic faults (PFs) or partial dislocations with $\frac{1}{6}\times\langle 2\bar{2}03\rangle$-type Burgers vectors (generally formed during island growth) [14,15] or by the formation of Shockley partials (which we call "geometrical partial MDs," or GPMDs). PFs do exist in sample 2, but they are always aligned roughly perpendicular to the steps. The $\frac{1}{6}\times\langle 2\bar{2}03\rangle$-type partials were rarely observed. Thus, GPMDs are the energetically favorable defects at the interface.

One of the advantages of VSE is that it may significantly enhance step-flow growth while suppressing island growth [13]. So the step-flow growth mode is assumed in Fig. 4(a). To see how the GPMDs are formed, let us consider the step marked with an arrow in Fig. 4(a). When this step advances to the right, it tends to change from *C* to *A* stacking positions in order to form the 2*H* structure. The transition may occur preferentially at the highly stressed steps [16,17]. As shown in Fig. 4(b), the transition is *gradual* and the layer keeps the hexagonal cells (indicated by the connecting lines) in the transition region although with some distortions. Afterwards, all the subsequent layers above will occupy the stacking positions of the hexagonal cells of this layer. The final structure of the transition volume is a GPMD with Burgers vector $\mathbf{b} = \frac{1}{3}\langle 1\bar{1}00\rangle$ [18]. When the dislocation line is parallel to $[1\bar{1}00]$, the GPMD is a 60° or screw partial.

Because of lattice displacements near the GPMD, the stacking sequence above the GPMD is altered *with respect to the substrate coordinates,* although not in such a way that a vertical boundary is the result [19]. This can be seen more clearly in Fig. 4(c), which has been constructed by vertically translating the perfect 2*H* lattice far above a 60° GPMD down into the 6*H* coordinates. Here the lattice displacements around the GPMD core have been averaged as a slight change of the 2*H* lattice constant (strain relaxation). The resulting change in lattice registry corresponds to the transition from *ACAC*... to *BABA*... imparted by the GPMD. Thus, the entire epilayer in Fig. 4(a) is a single 2*H* structure without vertical boundaries.

Note that the formation of GPMDs is a geometrical requirement for correcting the mismatched stacking sequences at the vicinal 2*H*/6*H* interface. There may be other possible GPMD configurations, but Fig. 4(a) is the one that requires the minimum number of GPMDs. Under the condition that this configuration is maintained, 1/3 of the steps correspond to GPMDs. This means that the

GPMD density is *predetermined* by the offcut angle, independent of the lattice mismatch. For 3.5° offcut, the (one-bilayer) step spacing is 4.1 nm, corresponding to a GPMD spacing of 12.3 nm. Surprisingly, this value is in good agreement with the average spacing, ~11 nm, of 60° GPMDs measured in sample 2.

The orientations of the GPMD Burgers vectors are determined by the in-plane mismatch strains. Because $a_{\mathrm{AlN}} > a_{6H\text{-SiC}}$, the GPMDs at the AlN/SiC interface are predominantly 60° GPMDs with the extra half planes located in the substrate (Fig. 3). These GPMDs provide a natural mechanism for relaxation of mismatch strains. This implies that one can control the extent of strain relaxation by simply adjusting the offcut angle. Based on Fig. 4(a), there exists an optimal offcut angle φ_c that corresponds to the condition where the GPMDs alone can fully relax the mismatch. With $\Delta a/a \sim 1\%$ between AlN and 6*H*-SiC, the optimal angle is $\varphi_c = 2.8°$ [20]. For offcut angle $\varphi > \varphi_c$, some GPMDs will form as either screw partials or 60° partials with the extra half planes in AlN to compensate what would otherwise result in excess strain relief. For $\varphi < \varphi_c$, full strain relaxation requires the formation of additional MDs. However, the 60° GPMD spacing of 11 nm measured in sample 2 corresponds to a small degree of excess strain relief of AlN along $[11\bar{2}0]$. This may indicate a nonbiaxial strain state where the lattice is compressed along $[1\bar{1}00]$ (parallel to the interface steps), since the GPMDs along $[1\bar{1}00]$ relax only the $[11\bar{2}0]$ strains although some GPMDs may glide into other directions to relax strains along $[1\bar{1}00]$.

For the on-axis sample, the substrate surface roughness also gives rise to irregular steps, but the density is much lower. Then the strains are mainly relaxed by the formation of complete MDs, which requires extra energy. Consequently, the AlN epilayer is more strained than that on the off-axis SiC substrate, as verified in Fig. 1.

The formation of GPMDs is a unique property of heterostructures with different stacking sequences. The mismatch at the GaN/AlN interface is still relaxed by complete MDs or dissociated partials. The different strain states of the GaN epilayers obtained from the x-ray measurements are mostly attributable to the extents of relaxation at the AlN/SiC interfaces of our samples. Experiments show that surface steps of nitrides along $\langle 1\bar{1}00\rangle$ usually develop into jagged steps during growth [21]. Since the *local* Nagai tilt is always perpendicular to the local step (see inset I of Fig. 2), the jagged steps can give rise to small Nagai tilt splitting, which then provides a driving force for the formation of MDs. This mechanism might provide an additional relaxation process at vicinal GaN/AlN interfaces.

Plan-view TEM observation also shows that the TD densities in the GaN epilayers of samples 1 and 2 are $\sim 5 \times 10^9$ and $\sim 8 \times 10^8$ cm^{-2}, respectively, consistent with the x-ray FWHM values. TDs in nitrides are generally formed in coalescence of misoriented islands [22]. The lower TD density in sample 2 supports the fact that VSE can suppress island formation through step-flow growth [13,21]. The relief of high stresses may also help suppress the formation of TDs [17].

In summary, VSE of nitrides on SiC has been demonstrated to facilitate rapid relaxation of mismatch strains at the interfaces. The strains were found to be relaxed mainly by unpaired GPMDs that must form to correct the different stacking sequences between the 2*H* and 6*H* structures. This mechanism indicates that strain relaxation can be controlled by adjusting the substrate offcut angles and directions (the latter may result in zigzag steps [21,23] that can relax strains two dimensionally). This ''step-controlled-epitaxy'' strategy may be developed to overcome the mismatch problem of nitride epitaxy on dissimilar substrates.

This work was supported by ONR MURI on III-Nitride Crystal Growth and Wafering, Grant No. N00014-01-1-0716 (monitored by Dr. C. Wood). Synchrotron diffraction was performed at beamline X19C of NSLS, BNL, which was supported by the U.S. DOE under Contract No. DE-AC02-98CH10886.

*Electronic address: xiahuang@ms.cc.sunysb.edu

[1] S. Einfeldt, Z. J. Reitmeier, and R. F. Davis, J. Cryst. Growth **253**, 129 (2003).
[2] T. W. Warren, Jr. *et al.*, Appl. Phys. Lett. **67**, 401 (1995).
[3] M. H. Xie *et al.*, Appl. Phys. Lett. **77**, 1105 (2000).
[4] J. Kato *et al.*, Appl. Phys. Lett. **83**, 1569 (2003).
[5] L. Lu *et al.*, Semicond. Sci. Technol. **17**, 957 (2002).
[6] X.-Q. Shen, M. Shimizu, and H. Okumura, Jpn. J. Appl. Phys. **42**, L1293 (2003).
[7] A. Bauer *et al.*, Phys. Rev. B **57**, 2647 (1998).
[8] M. Leszczynski *et al.*, Appl. Phys. Lett. **69**, 73 (1996).
[9] H. Nagai, J. Appl. Phys. **45**, 3789 (1974).
[10] X. R. Huang *et al.*, Appl. Phys. Lett. **86**, 211916 (2005).
[11] F. Riesz, J. Vac. Sci. Technol. A **14**, 425 (1996).
[12] R. Beanland and R. C. Pond, Inst. Phys. Conf. Ser. **104**, 455 (1989).
[13] T. Kimoto, A. Itoh, and H. Matsunami, Phys. Status Solidi A **202**, 247 (1997).
[14] P. Vermaut *et al.*, Philos. Mag. A **75**, 239 (1997).
[15] B. N. Sverdlov *et al.*, Appl. Phys. Lett. **67**, 2063 (1995).
[16] F. Riesz, Surf. Sci. Lett. **292**, L817 (1993).
[17] A. G. Cullis, A. J. Pidduck, and M. T. Emeny, Phys. Rev. Lett. **75**, 2368 (1995).
[18] With the 2*H* structure as the reference, the GPMDs bound ''natural,'' preexisting semi-infinite stacking faults in the 6*H* substrate.
[19] J. P. Hirth and J. Lothe, *Theory of Dislocations* (Krieger, Malabar, 1982), p. 314.
[20] For GaN/6*H*-SiC interfaces ($\Delta a/a \sim 3.5\%$), the optimal offcut is 9.7° according to the model in Fig. 4(a).
[21] M. H. Xie *et al.*, Phys. Rev. Lett. **82**, 2749 (1999).
[22] B. Moran *et al.*, J. Cryst. Growth **273**, 38 (2004).
[23] V. Ramachandran *et al.*, J. Electron. Mater. **27**, 308 (1998).